Porosity and Pore Area Determination of Hollow Fiber Membrane Incorporating Digital Image Processing

[a]MOHAMMAD ABBASGHOLIPOURGHADIM,[a*]MUSA MAILAH, [a]INTAN ZAURAH MAT DARUS, [b]A. F. ISMAIL, [b]M. REZAEI DASHTARZHANDI, [c]MEHDI ABBASGHOLIPOURGHADIM, [a]SHAHAB KHADEMI
[a]Faculty of Mechanical Engineering, [b]Advanced Membrane Technology Research Centre
Universiti Teknologi Malaysia, 81310 UTM Skudai, Johor Bahru
MALAYSIA
[c]Islamic Azad University, Bonab, East Azarbayjan
IRAN
amohammad27@live.utm.my, musa.mailah@gmail.com, intan@fkm.utm.my, afauzi@gmail.com, rdamasood1159@gmail.com, m.a_pour@yahoo.com, shahab.mech@gmail.com

Abstract:- Hollow Fiber Membrane (HFM) surface properties are crucial factors for evaluating the membrane performance in a specific application. Hence, this study aims to introduce an attractive and convenient method of calculating the membrane surface pore area, pore distribution and surface porosity. The results also suggest how to control the spinning conditions towards fabricating a suitable membrane based on the requirements of a process. The image processing package (IPP) changed the qualitative surface information from the outer surface via the field emission scanning electron microscopy (FESEM) images to quantitative results. The IPP determines the pore area, pore area distribution and surface porosity of membrane. The calculated surface porosity of the membranes was compared with the achieved value obtained from the gas permeation test. There was no significant difference between the results of both methods, thereby confirming the applicability of IPP for the study of membrane surface properties. This work presents a novel approach to evaluate the pore size, pore area and surface porosity of HFM for various conditions.

Key-Words:- Hollow fiber membrane, Image processing, Pore area, Pore area distribution, Surface porosity

1 Introduction

The study of membrane morphology generally is related to the properties of the membrane surface [1]. The porosity, pore size and pore size distribution of the membranes can be obtained by several methods. They include molecular weight cut-off (MWCF) method [2], pressure of bubbles approach [3], field emission scanning electron microscopy (FESEM) [4], scattering the X-ray with small angle [5], atomic force microscopy (AFM) technique[6-7], mercury intrusion method [8], liquid–liquid or liquid-gas displacement approach [9] and gas permeation test [10]. Image processing is a new and convenient method which is able to determine the membrane properties such as pore size, pore size distribution and porosity by digital analyzing. The dimension, shape and the number of pores in a special area of a membrane can be inspected by image processing analysis.

Pereira studied the surface properties of the HFMs by applying digital image processing [11]. The authors then compared the results with those obtained from scanning electron microscopy (SEM). First, the images were converted to grey scale and then to binary images by thresholding. The images were then partitioned into black and white pixels. Eventually, the porosity of membrane was determined by image structure analyser in 3D [11]. However, they did not classify the pore sizes on the surface of the membranes which may decrease the accuracy of the obtained porosity.

Surface porosity, pore size and pore size distribution were determined in this paper by dealing with the FESEM images of the membranes using a digital IPP package and the results were then further compared with the achieved results from gas permeation test.

2 Experimentation

A detailed description of the experimentation carried out in the study is described in the following sections.

ISBN: 978-1-61804-298-9

2.1 Membrane Preparation

Commercial *Polysulfone* (PSf) polymer pellets (1700) were supplied by Arkema Inc., PA, USA. *1-Methyl-2pyrrolidone* (NMP) and *Polyvinylpyrrolidone K90* (PVP) were used as solvent and non-solvent additives in the polymer solution dope. The composition of the fabricated membranes is given in Table 1.

Table 1: Composition of fabricated membranes

Composition	Density of Composition (g/cm^3)	Weight of Composition (g)	Volume of Composition (cm^3)	Density of Solution (g/cm^3)
Polysulfone (PSf)	1.2	180.0	145.2	1.1
N-Methyl-2-pyrrolidone (NMP)	1.0	790.8	767.6	
Polyvinylpyrrolidone (PVP)	1.2	30.1	25.1	
		1000.9	938.0	

The materials were dried in a vacuum oven for 48 hours at 80±2 ^{o}Ċ to remove the moisture. HFMs were prepared by the combination of the wet-phase inversion method and the solution dispersion technique as described elsewhere [12]. PVP was first added to the solvent (NMP) under vigorous stirring. The PSf polymer (18%) was then gradually added to the mixture with stirring done simultaneously. The prepared solutions were degased by ultra-sonication and loaded into a storage tank. The dopes were sent to the spinneret by pressurized Nitrogen (N_2). Distilled and tap water were used as bore fluid and external coagulant, respectively. The membranes were fabricated at different dope extrusion and bore fluid rates. They were then immersed in water for 72 hours to remove the residual solvent and non-solvent. Table 2 lists the specific details of the spinning conditions.

Table 2. HFMs spinning conditions

Dope extrusion rate (mL/min)	2-4.7
Bore flow rate (mL/min)	0.7-1.6
Bore composition (wt%)	Distilled water
External coagulant	Tap water
Air gap distance (cm)	0
Collection drum speed (m/min)	2.8
Spinneret OD/ID (mm)	1.1/0.55
Spinning dope temperature ($^{\circ}$C)	ambient
External coagulant temperature ($^{\circ}$C)	ambient
Bore fluid temperature ($^{\circ}$C)	ambient

2.2 Gas Permeation Test, Pore Size and Porosity

The pore size and surface porosity to study mass transfer rate of the porous asymmetric membranes in gas-liquid contacting processes are crucial and of great importance. Three modules were prepared for each type of membranes containing one hollow fiber with an effective length of 10 cm to obtain results that are more accurate. The hollow fibers were glued with epoxy glue at one end and the other end was potted to a stainless steel fitting. Purified nitrogen gas was supplied through the shell side of the modules and the N_2 pressure was increased at an interval of 0.5 bar. The permeation rates of gas coming out from the lumen side were measured by a soap-bubble flow meter. Each module was tested once and the average permeation rates were reported. The overall gas permeation through porous HFMs is assumed to be a combination of *Poiseuille* (P_P) and *Knudsen* (P_K) flow regimes which by further assumption of straight and cylindrical pores, the total permeance is given by [13]:

$$J_{total} = \frac{F_{total}}{A\Delta p} = \varepsilon \frac{1}{lRT}\left[\frac{r^2}{8\eta}\bar{p} + \frac{2r}{3}\left(\frac{8RT}{\pi M}\right)^{1/2}\right] \quad (1)$$

where J_{total} is the total gas permeance (mol m^{-2} Pa^{-1} s^{-1}), R is the universal gas constant (8.314 J mol^{-1} K^{-1}), T is the absolute temperature (K), M is the molecular weight of gas (kg mol^{-1}), r is the mean pore radius (m), η is the viscosity of gas (Pas), ε is the surface porosity (A_p/A_T where A_p is the area of pores and A_T is the total area of membrane), l is the effective pore length (m) and $\bar{p}$ is the mean pressure (Pa) $(p_u + p_d)/2$ where p_u is the upstream pressure and p_d is the downstream pressure. The permeance can be determined by measuring the gas permeation

ISBN: 978-1-61804-298-9

rate under a certain pressure difference across the membrane.

$$J_{total} = a\bar{p} + b \quad (2)$$

The values of a and b can be determined from the intercept and slope respectively in the J_{total} versus p plot [13]. The mean modal pore radius is calculated by:

$$r = \frac{16}{3}\left(\frac{a}{b}\right)\left(\frac{8RT}{\pi M}\right)^{1/2}\eta \quad (3)$$

The effective surface porosity over the effective pore length ε/l can thus be calculated as follows:

$$\frac{\varepsilon}{l} = \frac{8\eta RT}{r^2} \quad (4)$$

Note that the effective pore length (l) is difficult to measure in practice and it is in fact not necessary to measure. Instead, it is convenient to use a combined parameter ε/l representing the porous structure of the membrane.

3 Field Emission Scanning Electron Microscopy (FESEM)

The membranes were put in holders and coated by sputtering platinum. A *Zeiss Supra 35VP* field emission scanning electron microscope (FESEM) with EDX analysis, from Carl Zeiss, Inc., (MN, USA) was used to observe the outer surface of the fabricated membranes.

4 Image analyses (Pre-processing)

Generally, the grey images from the outer surface of a porous membrane is between zero and 255 pixels in which, pixels with low and high luminance were assumed as pore areas and background, respectively. In the first step, the FESEM images were resized into 1000×1000 square pixels in order to transfer to the computer for analysis. For filtration, the *medfilt2* function was used to eliminate the noises from the colour images. Then *Unsharp* algorithm was used to increase the intensity of the images and edges. Before classification, the images were adjusted as red green blue (RGB) images to detect the pore boundaries clearly. The surface porosity of fabricated membranes was calculated by the following equation:

$$\varepsilon = \frac{\int_0^h (Ap)_z dz}{(At)} \quad (5)$$

where At is the total area of image, Ap is the area porosity at distance z, h is height of image. To obtain accurate results, three modules for each membrane type were prepared. The results were averaged and the mean surface porosity of the three modules was assumed.

4 Results and Discussion

The results obtained from the study is analyzed and discussed in the following subsections.

4.1 Field Emission Scanning Electron Microscopy (FESEM) and Image Analyses (Pre-processing)

Fig. 1 (a) shows FESEM surface micrograph of fabricated membrane. The FESEM images that qualitatively give the pore size, pore size distribution and the porosity of the membrane surface was adjusted to give the best threshold. In fact, it is difficult to extract the exact pores with the same threshold for various FESEM images of the HFMs. Hence, the triangle algorithm was extended to find on which side of the maximum peak the data goes the furthest and searches for the threshold within that largest range. The time of exposure, lighting and smooth or unsmooth outer surface of HFM are the significant criteria for adjusting the threshold. The FESEM micrograph after adjusting can be seen in Fig. 1(b).

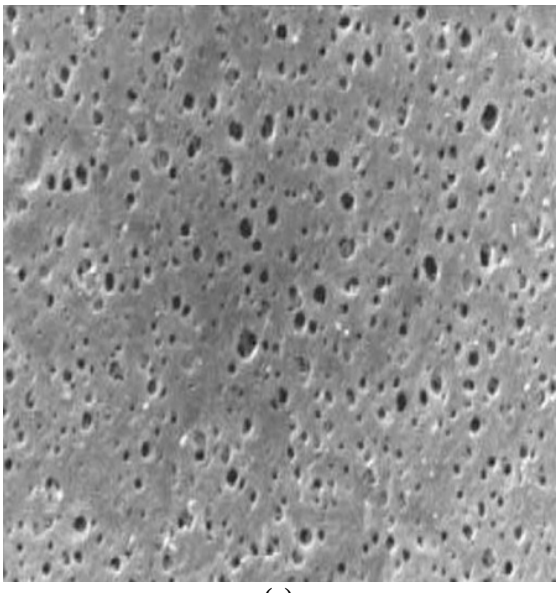

(a)

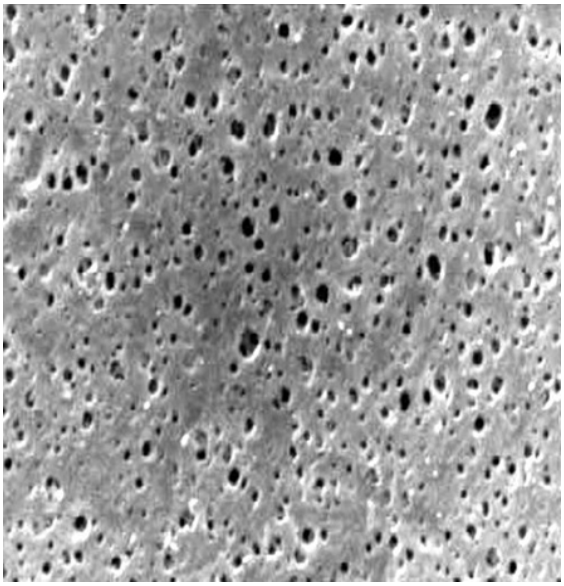

(b)

Fig. 1: FESEM outer images (a) original image; (b) adjusted image

It can be clearly observed that the boundary of pores are more visible in Figure 1(b) in comparison to the original FESEM image which makes easier extraction of the pores for further analysis in later sections. Knowingly, all the black colors in FESEM images cannot be assumed as real pores. Hence, the existence of pores in images should be extracted and then classified. The classified pores of the outer membrane surface by triangle algorithm are illustrated in Figure 2.

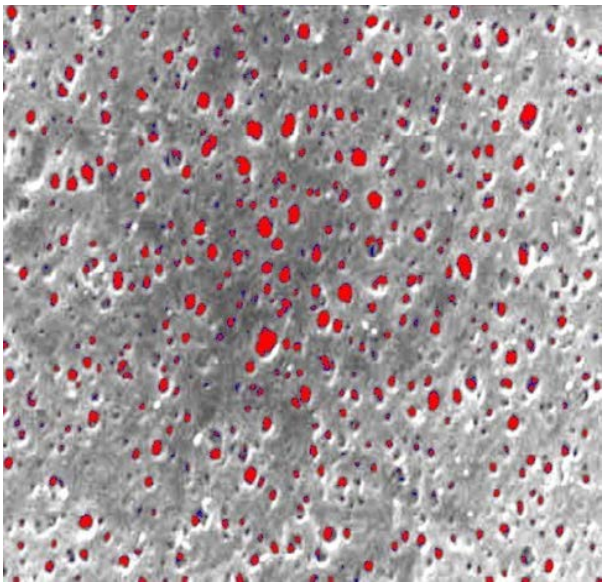

Fig. 2: Pore extraction process of membrane outer surface by triangle algorithm

After the pore classification, two groups of membrane pore could be easily detected from Figure 2. First, the main and real pores that are separated with red color. Secondly, the blue color pores which assumed as failed pores. Since only the real pores are needed to determine the pore size, pore size distribution and surface porosity, the failed pores were ignored and the final extracted image was converted to binary images by data analyzing result which can be seen in Figure 3.

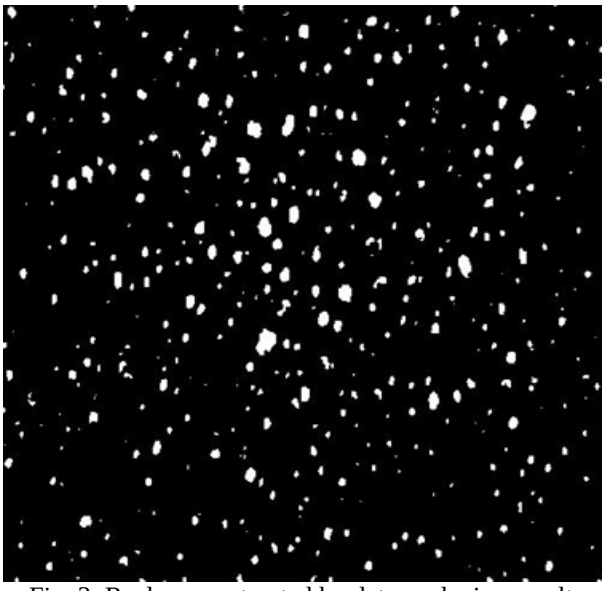

Fig. 3: Real pore extracted by data analyzing result

The white color objects in Figure 3 are the final real pores extracted from Figure 1 (a) and the black part is the surface of the membrane with no pores. The area and distribution of the membrane surface pores will be calculated in the next section based on this figure.

4.1 Pore Size Distribution

The *bwlabel* and *regionprops* functions were used to determine the pore size distribution and area based on the achieved binary image. The digital data after analyzing them is shown in Figure 4.

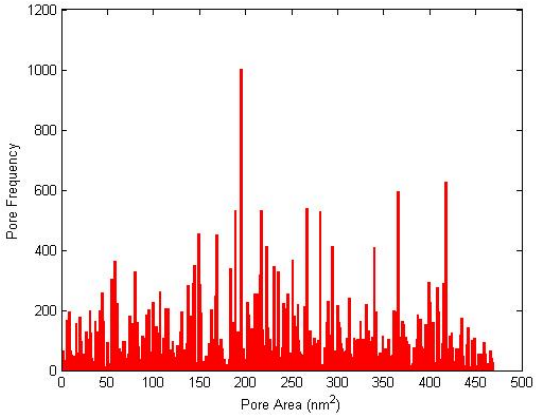

Fig.4. Data showing the result of pore area distribution

ISBN: 978-1-61804-298-9

The number of pores as well as their size can be extracted from the figure. This can help to modify the membrane surface towards a specific application.

4.2 Surface Porosity

The surface porosity of HFMs was obtained by gas permeation test (GPT) and our image processing package (IPP) (see Table 3). From the table, it is revealed that the surface porosity decreases with an increase in DER. This might be ascribed to the fact that the stress inside the spinneret increases by increasing the extrusion rate of solution. In addition, it can be detected as well that the obtained results from both methods are not too dissimilar which can confirm the applicability of image processing method for porosity determination.

Table 3. Surface porosity of different fabricated HFMs analyzed by GPT and IPP

HFM NO.	DER cm^3/min	BFR cm^3/min	CD	Porosity by GPT %	Porosity by IPP %
1	2.0	0.7	1.5	**8.3**	**8.92**
2	2.3	0.8	1.6	**7.9**	**8.11**
3	2.6	0.9	1.7	**7.8**	**7.63**
4	2.9	1.0	1.8	**6.9**	**7.23**
5	3.2	1.1	1.9	**6.7**	**7.56**
6	3.5	1.2	2.0	**6.6**	**7.04**
7	3.8	1.3	2.1	**6.4**	**6.89**
8	4.1	1.4	2.2	**6.0**	**6.45**
9	4.4	1.5	2.3	**5.8**	**6.21**
10	4.7	1.6	2.4	**5.7**	**5.94**

DER: Dope extrusion rate; BFR: Bore fluid flow rate

5 Conclusions

In the present work, a system was designed to measure the membrane surface porosity, pore area distribution by detecting the changes of the pixel inside the FESEM images. PSf HFMs in different spinning conditions were spun and the real pores were extracted successfully from the original FESEM images of the HFMs. Then the area and distribution of the pores were calculated based on the image processing package. The surface properties were further determined by GPT and IPP methods. The results for both calculated and actual approaches were close, and hence confirming the applicability of the method for calculating surface porosity.

Acknowledgements

We would like to thank the Malaysian Ministry of Higher Education (MOHE) and UTM for providing the research funding and facilities. The research is executed using Vote No.: Q.J130000.2513.02H15.

References:

[1] Rezaei, M., A.F. Ismail S.A. Hashemifard, G. Bakeri and T. Matsuura, "Experimental study on the performance and long-term stability of PVDF/montmorillonite hollow fiber mixed matrix membranes for CO 2 separation process", I*nternational Journal of Greenhouse Gas Control*, Vol. 26, pp. 147-157, 2014.

[2] I. Okazaki, H. Ohya, S.I. Semenova, S. Kikuchi, M. Aihara and Y. Negishi, "Nanotechnological method to control the molecular weight cut-off and/or pore diameter of organic–inorganic composite membrane", *Journal of Membrane Science*, Vol. 141, No. 1, pp. 65-74, 1998.

[3] F. Vigo, A. Bottino, S. Munari and Gustavo Capannelli, "Preparation of asymmetric PTFE membranes and their application in water purification by hyperfiltration", *Journal of Applied Polymer Science*, Vol. 21, No. 12, pp. 3269-3290, 1977.

[4] Wang, L. and X. Wang, "Study of membrane morphology by microscopic image analysis and membrane structure parameter model", *Journal of Membrane Science*, Vol. 283, No. 1, pp. 109-115, 2006.

[5] Yang, B. and A. Manthiram, "Comparison of the small angle X-ray scattering study of sulfonated poly (etheretherketone) and Nafion membranes for direct methanol fuel cells", *Journal of Power Sources*, Vol. 153, No. 1, pp. 29-35, 2006.

[6] Bowen, W.R. and T.A. Doneva, "Artefacts in AFM studies of membranes: correcting pore images using fast fourier transform filtering", *Journal of Membrane Science*, Vol. 171, No. 1, pp. 141-147, 2000.

[7] Stamatialis, D.F., C.R. Dias, and M.N. de Pinho, "Atomic force microscopy of dense and asymmetric cellulose-based membranes", *Journal of Membrane Science*, Vol. 160, No. 2, pp. 235-242, 1999.

[8] Sing, K.S. and S. Gregg, *Adsorption, surface area and porosity*. Academic Press, London, 1982.

[9] K.S. McGuire, K.W. Lawson and D.R. Lloyd, "Pore size distribution determination from liquid permeation through microporous membranes", *Journal of Membrane Science*, Vol. 99, No. 2, pp. 127-137, 1995

[10] Rezaei, M., A.F. Ismail, G. Bakeri, S.A. Hashemifard and T. Matsuura, "Effect of general montmorillonite and Cloisite 15A on structural parameters and performance of mixed matrix membranes contactor for CO2 absorption", *Chemical Engineering Journal*, Vol. 260, No. 0, pp. 875-885, 2015.

[11] Pereira, C., R. Nobrega, and C. Borges, "Spinning process variables and polymer solution effects in the die-swell phenomenon during hollow fiber membranes formation", *Brazilian Journal of Chemical Engineering*, Vol. 17, No. 4-7, pp. 599-606, 2000.

[12] Rezaei, M., A.F. Ismail, S.A. Hashemifard and T. Matsuura, "Preparation and characterization of PVDF-montmorillonite mixed matrix hollow fiber membrane for gas–liquid contacting process", *Chemical Engineering Research and Design*, Vol. 92, No. 11, pp. 2449-2460, 2014.

[13] Wang, D., K. Li, and W. Teo, "Porous PVDF asymmetric hollow fiber membranes prepared with the use of small molecular additives", *Journal of Membrane Science*, Vol. 178, No**.** 1, pp. 13-23, 2000.

ISBN: 978-1-61804-298-9